Volume 18, No 1 | International Journal of Radiation Research, January 2020

Non-rigid magnetic resonance image registration for cervical cancer radiation therapy evaluation using hybrid features

L. Zhi[1,2], S. Zhang[1,2*], J. Xin[3], J. Ma[3], R. Zhu[2]

[1]*School of Computer Science and Engineering, North Minzu University, Yinchuan 750021, China*
[2]*Department of Radiology, People's Hospital of Ningxia Hui Autonomous Region, Yinchuan, 750021, China*
[3]*Department of Radiology, Shengjing Hospital of China Medical University, Shenyang, 110022, China*

► ***Original article***

Corresponding authors:
Zhang Shaomin, PhD.,
Fax: *+86 0951 206 6511*
E-mail:
shmzhang_paper@163.com

Revised: April 2019
Accepted: May 2019

Int. J. Radiat. Res., January 2020; 18(1): 13-22

DOI: 10.18869/acadpub.ijrr.18.1.13

ABSTRACT

Background: A non-rigid cervical magnetic resonance (MR) image registration algorithm combining pixel intensity and local region gradient features was proposed in this study for cervical cancer radiation therapy (RT) evaluation. ***Materials and Methods:*** The method was based on the following main steps: (1) each patient was scanned 2 times. The first scan was before internal-beam RT, and second scan was about 3~4 weeks after internal-beam RT. (2) DoG salient points mixed with stochastically sampled points were used as keypoints, and pixel intensity and PCA-SIFT features around them were extracted to build a feature vector for each keypoint. (3) In non-rigid registration process, α-mutual information (α-MI) was used as similarity measure. The method was evaluated by 20 MR images acquired from 10 patients with biopsy-proven squamous cell carcinomas. ***Results:*** For cervical cancer, the deformation of tumor and organ between different MR image acquisitions was subject to several errors, including possible mechanical misalignment, respiratory and cardiac motion, involuntary and voluntary patient motion, bladder and bowel filling differences. To minimize these ambiguities, patients filled their bladder before scanning. The proposed hybrid features can effectively catch the bladder and bowel in MR images, and α-mutual information (α-MI) based non-rigid registration can effectively align two long time internal MR images. ***Conclusion:*** Non-rigid cervical MR image registration method using hybrid features on α-MI can effectively capture different tissues in cervical MR images. Accurately aligned MR images can assist cervical cancer RT evaluation process.

Keywords: *Cervical cancer radiotherapy evaluation, magnetic image registration, hybrid feature, pca-sift, α-mutual information.*

INTRODUCTION

Cervical cancer is one of the leading causes of cancer death in women worldwide, with an estimated incidence of more than 528000 new cases in 2012, and 266000 women died of the disease[1]. For the locally advanced stage of disease, radiation therapy (RT) is the standard treatment, which includes external-beam and internal-beam radiation. MR imaging is now widely accepted as the reference imaging modality for detection of local spread of cervical cancer with its superior soft-tissue resolution. MRI is also an effective modality for monitoring the tumor response to therapy before, during and after radiation therapy [2, 3]. In our cooperative hospital and according to the treatment protocol, each patient usually underwent MR scans for 2 times: the first time was before internal-beam radiation therapy, and the second time was about 4 weeks after internal-beam radiation therapy. Follow-up T2-

[Downloaded from ijrr.com on 2026-11-24]

[DOI: 10.18869/acadpub.ijrr.18.1.13]

weighted and diffusion-weighted MRI of cervical cancer may provide information of distinguishing recidivistic tumor from radiation induced fibrosis changes during RT treatment [2].

However, in cervical cancer, the deformation of tumor and organ (bladder and rectum filling differences) between different MR image acquisitions presents significant challenges for the accurate evaluation of the tumor response to therapy. To overcome these problems, anatomical changes need to be managed by non-rigid registration. Image registration consists of establishing spatial correspondences between different images, which plays a fundamental role in medical image analysis. Some typical important applications include: 1) diagnosis, where image information fused from different imaging devices or protocols is used in facilitating the diagnosing process; 2) radiation therapy, where images acquired at different times or even in different modalities are employed in gross tumor volume (GTV) delineation and treatment planning; 3) image-based quantitative analysis often needs high precision registration between medical images. Among these, deformable (also called nonrigid or elastic) registration has been one of the main challenges that have drawn a lot of attention from researchers.

Medical images can be aligned by evaluating a criterion based on the whole image intensities, by establishing of correspondences between landmarks, or by a hybrid method combining the previous two methods. Information theoretic similarity measures are commonly used in medical image registration. These measures include Mutual Information (MI), Normalized Mutual Information (NMI), Kullback-Leibler Divergence (KLD), Jensen-Shannon Divergence (JSD), Renyi Entropy (RE) also called α-MI and so on. When aligning two images based on correspondences between two subsets of image voxels, three steps are usually followed. First, interesting point's detection; second, features extraction, and then correspondences establishment. Harris, Hessian and DoG are customarily selected as salient points. As for features, many invariant descriptors have been developed[4]. Among them, SIFT, PCA-SIFT, GLOH, SURF have been applied in medical imaging, and have gotten success in some contexts[5, 6].

Compared with head and neck, and lung, registration of images in the pelvic region is challenged by the large and complex organ and tumor deformation [7]. Very limited work has been reported to cervical MRI registration. In the early stage, landmarks marked by hand were used to represent the anatomical structure and register images from different scans or modalities. Ferris et al. [8] used a small round paper dot in the cervix to align colposcopic image. However, the location of the landmarks may shift during the scan, resulting in inaccurate registration results. Osorio et al.[9] proposed a nonrigid registration framework for radiation treatment of cervical cancer. First, the structures of the bladder, the rectum and the cervix uterus were manually delineated on axial CT scans. Then, control points were generated from the surfaces for each structure. Finally, the transformation between the control points in two CT scans was estimated. Lu et al.[10] focused on the problem of the deformation of the tumor in the MRI guided cervical cancer radiation therapy. First, the bladder and uterus were manually segmented for the therapy planning as a priori knowledge. Then, the segmentation and non-rigid registration were performed on the MR images during the course of the treatment. On the other hand, due to subjective and operator dependent of the Manual localization of landmarks, García-Arteaga *et al*. [11] presented to automatically extract and match landmarks from the colposcopical image sequences. First, they chose one frame of a colposcopical sequence as the template frame, and aligned all frames to the common template frame by a rigid transformation. Second, Harris points were detected in the roughly aligned images, and color and textural features were extracted around the Harris points over a 7×7 window. Finally, they performed non-rigid registration based on B-spline. Staring *et al*. [12] chose the set of Cartesian image structure features to perform registration of cervical MRI.

In this paper, we implemented a hybrid method combining pixel intensity and local

[Downloaded from ijrr.com on 2026-11-24]

[DOI: 10.18869/acadpub.ijrr.18.1.13]

region gradient features. Specifically, we employed DoG salient points mixed with stochastically sampled points, extracted pixel intensity and PCA-SIFT features around them to build a feature vector for each point. Based on them, α-MI was used as similarity measure during non-rigid registration process.

This study aimed to evaluate cervical cancer radiation therapy by using a new non-rigid MRI registration method with hybrid features.

MATERIALS AND METHODS

Patient selection

This study was carried out with approval by the local institutional research ethics committee (IREC) (Shengjing Hospital of China Medical University, Shenyang, China). The proposed method is evaluated on cervical MRI datasets of 10 patients with biopsy-proven squamous cell carcinomas. These patients' mean age was 51.6, range from 33-66. Among 30 to 39 cohort there was 1 patient, among 40 to 49 cohort there were 3 patients, among 50 to 59 cohort there were 4 patients, among 60 to 69 cohort there were 2 patients. The FIGO stages of these cases were spread from IIA to IIIB. The primary tumor MR volumes spread from 6.60 to 109.88 cc. Table 1 details the clinical characteristics of the 10 patients.

Image acquisition

The diagnostic MR scans were acquired with 16-channel phased array Torso coil. The diagnostic MR T2w scans parameters in the transversal direction are summarized in Table 2. Each patient was scanned 2 times. The first scan was before internal-beam radiation therapy, and second scan was about 3~4 weeks after internal -beam radiation therapy.

Table 1. Patient and tumor characteristics.

Characteristic	Value
Age	
Mean (SD) [median]	51.6 (8.8) [52.5]
Range	33-66
FIGO stage, n (%)	
IIA	1 (10)
IIB	6 (60)
IIIA	1 (10)
IIIB	2 (20)
Primary tumor MR volume, cc	
Mean (SD) [median]	35.90 (31.64) [23.79]
Range	6.60-109.88

Table 2. Sequence parameters of MRI scans.

	TR (ms)	TE (ms)	Slice thickness/ gap between slices (mm)	Matrix	FoV (mm)	Scan time (min)
T1 atMR FFE	4.1	2.3	6.0/0.0	320´320	600	01 : 06
T1 TSE axial	680	10	5/1	384´384	351	05 : 43
T2 TSE axial	5299	90	5/1	960´960	340	04 : 32
T2 TSE sagittal	5066	90	5/1	560´560	200	02 : 22
T2 TSE coronal	2522	100	5/0.4	400´400	350	01 : 03
T2 TSE SPAIR axial	10364	85	5/1	720´720	349	04 : 09
T2 TSE SPAIR sagittal	3600	70	5/1	640´640	220	02 : 31

Hybrid feature extraction

In this study, a combination of SIFT based on DoG points and pixel intensity in a compact form by using PCA feature dimension reduction method. Thus, the hybrid feature is used for cervical MRI in an efficient and effective way, which plays a key step in subsequent registration.

Tissue structure feature point detection

Gaussian scale space

Scale invariant region detectors have been successfully applied in computer vision area [13]. For medical image analysis, scale-space salient region-based features have also shown some advantages in tissue and anatomical structure representation [6]. A formal accepted scale-space

[Downloaded from ijrr.com on 2026-11-24]

[DOI: 10.18869/acadpub.ijrr.18.1.13]

theory for image processing is Lindeberg's Gaussian scale-space (also called linear scale-space) [14]. The Gaussian scale-space of an image is built by convolving the image I(x,y) with a variable-scale Gaussian kernel G(x, y, σ). The Gaussian kernel is the only filter that can be used to generate a linear scale-space, based on the essential requirement that new structures must not be created when going from a fine scale to any coarser scale [14].

Salient point/region detection

Lindeberg proposed that choosing local maximum response of scale-normalized Laplacian of Gaussian (LoG) can detect blob-like structures with proper size in an image [14]. Based on Lindeberg's work, Lowe improved blob structure detection process through a more practical way. In [15], Lowe used the difference of Gaussian (DoG) to build discrete image scale space, and detected local maxima and minima in a cubic 3×3 space at the current and adjacent scales. DoG function approximates to the scale-normalized LoG $\sigma^2 \nabla^2 G$. In practice, DoG keypoints not only tend to represent blob-like structures in an image, these points are also sensitive to pixels whose surrounding region has high intensity contrast and can detect some corner-like points. In cervical MRI, DoG points prefer to locate at edges of the bladder, bones and those tissues and structures with high intensity contrast. Figure 1 shows DoG points in cervical MRI of two subjects.

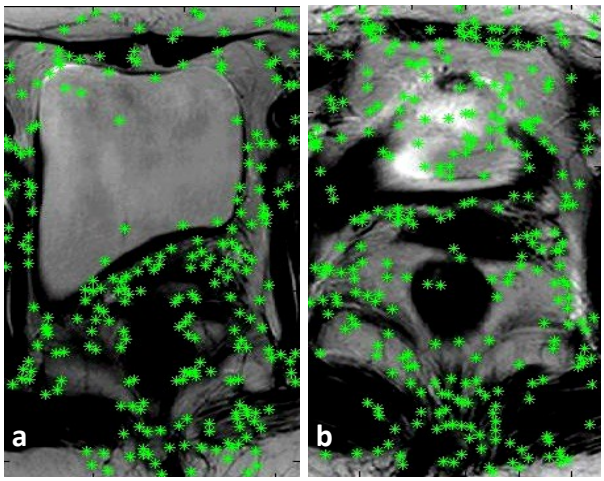

Figure1. Example of DoG points extracted from cervical MRI of two subjects.

Random points

In medical image registration, it is difficult to totally depend on automatic point detection. The number of feature points sometimes is unstable (for some images too large while for some too small), and the points tend to locate along the positions where intensity contrast is high. These factors may increase the error of registration. In Figure 1 (a), there are few DoG points inside the bladder and rectum area. In figure 1 (b), there are few DoG points inside the tumor area and rectum area. According to these, we add random points in order to increase the coverage on the area where intensity contrast is relatively low.

Pca-sift descriptor

Image gradient has always been a type of important feature for medical image registration [6]. If image feature is extracted around some salient points such as DoG points showed above, it is reasonable to use gradient information around these points to capture intensity contract information in the registration process. Scale Invariant Feature Transform (SIFT), is an image descriptor describing gradient distribution in a local neighborhood of a point. Mikolajczyk and Schmid revealed that SIFT descriptor got the highest rank under points' matching process[4].

Ke and Sukthankar further discussed that reduction dimension of standard SIFT descriptor by principal component analysis (PCA) can even get better results in image retrieval experiment with much less time during point matching process [16]. PCA-SIFT linearly projects high dimensional gradient patches centered to keypoints into low dimensional feature space.

PCA training process

The feature vector is built from gradient maps for the 41×41 keypoint patch, and the input vector for the training process has 2×39×39=3042 elements. The training process computes the eigenvalues and corresponding eigenvectors of a 3042-by-3042 covariance matrix built from selected patch gradient vectors of keypoint. Suppose X is the data matrix of keypoints with 3042 gradient patch, and X has

[Downloaded from ijrr.com on 2026-11-24]

[DOI: 10.18869/acadpub.ijrr.18.1.13]

been preprocessed as zero mean components. The matrix size is 3042-by-m, here m is the number of keypoints. The PCA training process consists of the following steps: (1) Making a 3042-by-3042 covariance matrix A by $A = XX^T$. (2) Computing eigenvectors: $e_1, e_2, e_3, \ldots e_n$, of the matrix A. (3) Choosing the top k eigenvectors to construct the projection matrix stored as a model file on disk.

For our data, in PCA training process, we extracted about 2000 DoG and random points from each cervical MR image. And computed the gradient patch centered at every point to form training vectors. The training process is detailed in Figure 2. The output of the training process is a model file which stores the projection matrix.

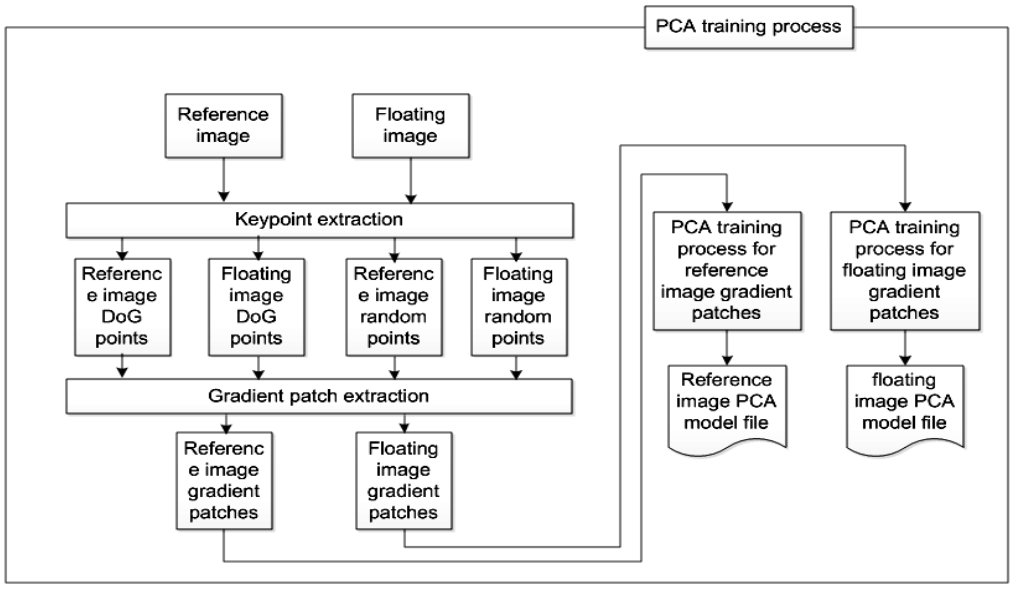

Figure 2. Training process of PCA.

When using the trained PCA eigenspace, we just input a 3042-element gradient vector of a given image patch and project it into k-dimension vector by matrix multiplication.

Building hybrid feature descriptors

As showed in Figure 1, local areas around DoG keypoints are appropriate for computing gradient-based descriptors, while for other tissues in cervical MRI that have low intensity contrast, pixel intensity has always been a reliable feature in registration. Based on these considerations, our descriptor contains pixel intensity and n-dimensional PCA-based gradient features, thus we get a new hybrid n+1 dimensional descriptor for all points in reference and floating images [g1,...,gn, i]. Here, gk is gradient feature and i is pixel intensity. Figure 3 is the main frame for building hybrid features.

Entropic spanning graph estimator based registration framework

Deformable registration process consists of establishing voxel-by-voxel correspondence through a nonlinear dense transformation or a spatially varying deformation model[6]. Mutual information (MI) is a widespread entropy-based dissimilarity measure. It has been successfully used in medical image registration, which does not assume any relationship between the image intensities[17]. Mutual information is generally calculated on pixel intensities by estimating a 2-dimensional joint histogram. However, the plug-in approaches that estimate high dimensional entropies are often troubled by the curse of dimensionality[18]. Redmond et al. proved that when a graph is continuous and "quasi-additive", the graph can be used to estimate the entropy directly[19]. Minimum

[Downloaded from ijrr.com on 2026-11-24]

[DOI: 10.18869/acadpub.ijrr.18.1.13]

spanning tree (MST) and k-Nearest Neighbor (kNN) graph are two frequently-used graphs for estimating α-entropies of feature probability density [20-22]. α-MI has already applied in medical image registration[12, 21]. In this work, we choose kNN-based α-MI for more efficient dealing with high-dimensional features. Figure 4 shows the flowchart of α-MI-based non-rigid image registration.

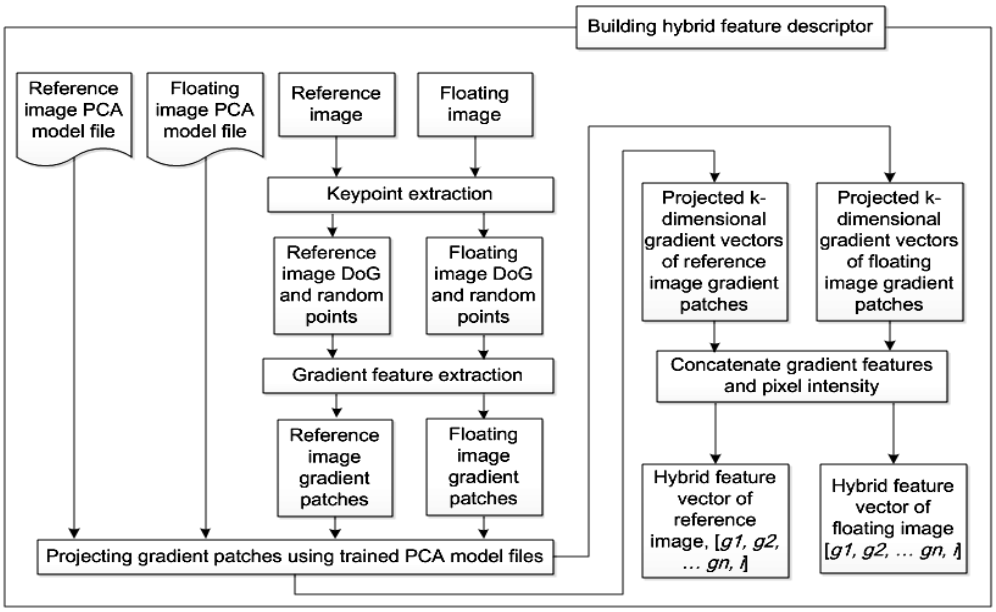

Figure 3. The main frame of building hybrid feature.

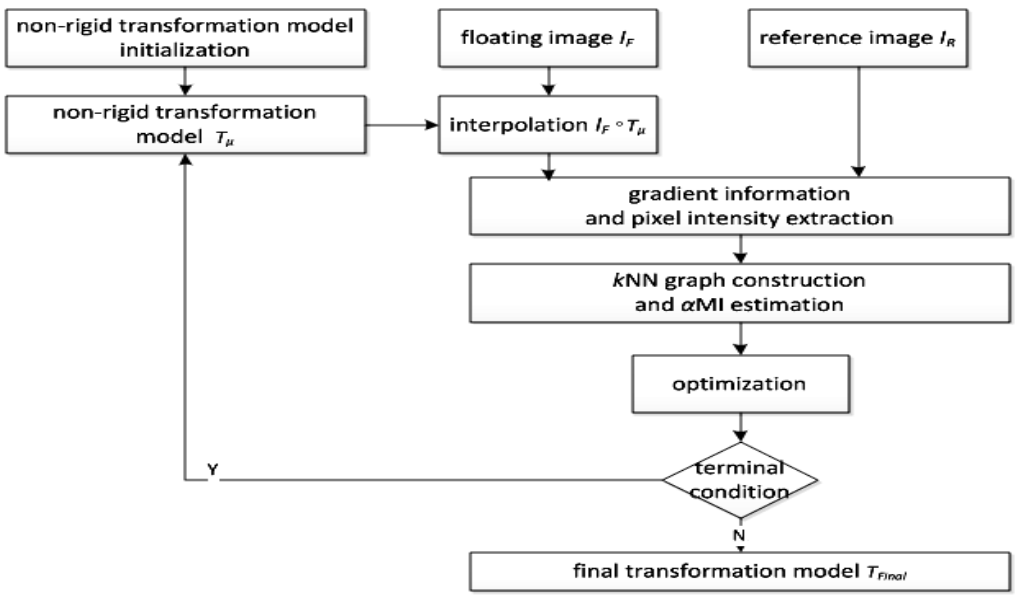

Figure 4. Algorithm flow diagrams.

[Downloaded from ijrr.com on 2026-11-24]

[DOI: 10.18869/acadpub.ijrr.18.1.13]

RESULTS

The proposed registration methods are implemented using public available medical image registration package Elastix [23] and a series of open source code in PCA-SIFT[16]. B-splines transformation is employed in this work by setting registration parameters in Elastix, feature extracting and training part are implemented by modified PCA-SIFT code which enables random point's descriptor building. All MR images are computed on a desktop computer with Inter Core i7-2600 CPU @ 3.4GHz and 4GB memory.

Experimental setup

In this work, we ran four experiments to explore the precision between different registration methods. One method is standard MI with 1-d pixel intensity. The other three methods are α-MI-based registration methods. (1) 1-d pixel intensity on MI (denoted as MI_pixel); (2) 1-d pixel intensity on α-MI (denoted as α-MI_pixel); (3) 1-d pixel intensity concatenated with PCA-SIFT (n=20) forms a 21-dimentional feature vector on α-MI (denoted as α-MI_pca-sift_21); (4) 1-d pixel intensity concatenated with PCA-SIFT (n=36) forms a 37-dimentional feature vector on α-MI (denoted as α-MI_pca-sift_37).

Evaluation measures

To evaluate the registration quality, Dice similarity coefficient (DSC) is used. This analysis is defined as equation 1:

$$\mathrm{DSC} = 2\frac{|\mathrm{A}\cap\mathrm{B}|}{|\mathrm{A}|+|\mathrm{B}|} \quad (1)$$

where, DSC value of 1 indicates perfect overlap, while a value of 0 indicates no overlap. The bladder and rectum were manually outlined by an experienced radiologist, in conjunction with the radiation oncologist in axial T2-weighted MRI for each image. The T2-weighted TSE and SPAIR images in axial and sagittal orientation were available to refine the delineation. In Dice formulation A was defined as segmented bladder (or rectum) of fixed binary image. B was defined as segmented bladder (or rectum) of moving binary image using transformation model after registration.

Experimental results and analysis

Table 3 and table 4 compare the DSC values of four registration methods. Results show that the best precision is achieved by α-MI_pca-sift_21. Figure 5a and b are reference image and floating image from the same patient, Figure 5c shows the checkerboard of the reference image and the deformed floating image using α-MI_pca-sift_21.

Table 3 and table 4 detail the results of four registration methods for the bladder and rectum of each patient respectively. From these two tables, we can see that α-MI_pixel (only pixel intensity with α-MI) is not a reliable registration method. In table 4, five cases (50% of all cases) performed poorly. When using the α-MI_pixel method, $z_R(x_i, y_i)$ may have the similar pixel intensity with its neighbor pixels($z_R(x_{ip}, y_{ip})$) and $\Gamma_i^R = \sum_{p=1}^{k} \left| z_R(x_i, y_i) - z_R(x_{ip}, y_{ip}) \right|$ may be too small of a value. The estimation of α-MI will become unstable when divided by a small number. For the other three methods, they perform fairly well. For bladder in Table 3, traditional MI_pixel (pixel intensity with MI) performs a little better (by 0.93% improvement) than α-MI_pca-sift_37. While for rectum in Table 4, α-MI_pca-sift_37 obviously exceeds traditional MI_pixel (by 5.7% improvement). Among these methods α-MI_pca-sift_21 gets the highest precision on both organs.

Generally, hybrid feature based methods have higher degree of overlap compared with α-MI_pixel and traditional MI_pixel. As for the length of reduced SIFT feature, it seems that large feature dimension may not get better performance. This observation was consistent with the experiment of Ke [16].

Patients were asked to fill their bladder before scanning. The volume of bladder in MR image is larger than that of rectum, and the movement of rectum between the two scans is larger than the movement of bladder. These may cause the registration precision of bladder to be better than rectum.

[Downloaded from ijrr.com on 2026-11-24]

[DOI: 10.18869/acadpub.ijrr.18.1.13]

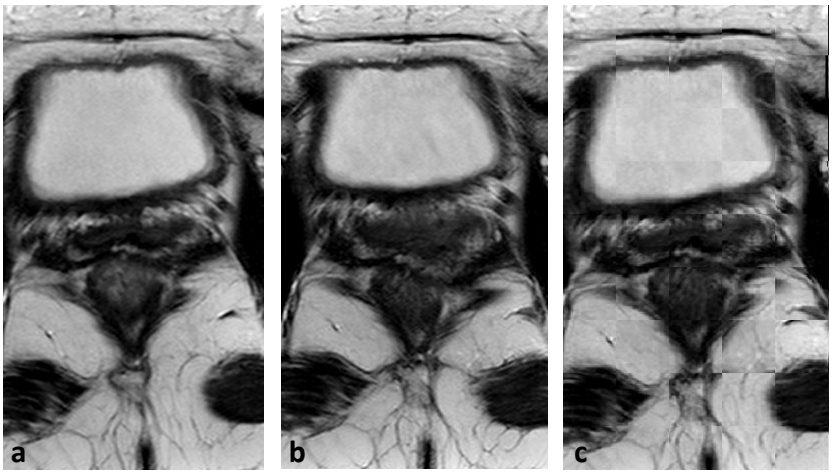

Figure 5. MR images of one subject, **(a)** Reference image **(b)** floating image **(c)** the checkerboard of the reference image and the deformed floating image using α-MI_pca-sift_21.

Table 3. The DSC values of four registration methods for the bladder.

Index	MI_pixel	α-MI_pixel	α-MI_pca-sift_21	α-MI_pca-sift_37
Pa1	0.650302	0.315849	0.698068	0.67445
Pa2	0.79046	0.656969	0.756952	0.742784
Pa3	0.859385	0.457219	0.868496	0.855465
Pa4	0.895165	0.776152	0.901129	0.879244
Pa5	0.780668	0.530721	0.837015	0.718078
Pa6	0.872489	0.890006	0.883953	0.873557
Pa7	0.713508	0.580031	0.722964	0.729837
Pa8	0.803228	0.143935	0.771377	0.784662
Pa9	0.777199	0.620969	0.779541	0.767119
Pa10	0.726168	0.408966	0.791333	0.771031
Mean value	0.786857	0.538082	**0.801083**	0.7796227

Table 3. The DSC values of four registration methods for the bladder.

Index	MI_pixel	α-MI_pixel	α-MI_pca-sift_21	α-MI_pca-sift_37
Pa1	0.576868	0.144611	0.570384	0.506882
Pa2	0.502071	0	0.367447	0.323442
Pa3	0.592313	0	0.582242	0.565482
Pa4	0.591575	0.561271	0.662204	0.697817
Pa5	0.525522	0.26043	0.543764	0.555376
Pa6	0.764006	0.761408	0.811032	0.840987
Pa7	0.045805	0	0.261051	0.290768
Pa8	0.709174	0	0.73449	0.713679
Pa9	0.701295	0.328523	0.756362	0.746964
Pa10	0.143573	0	0.36322	0.204279
Mean value	0.51522	0.205624	**0.56522**	0.5445676

[Downloaded from ijrr.com on 2026-11-24]

[DOI: 10.18869/acadpub.ijrr.18.1.13]

DISCUSSION

This study shows that the proposed algorithm provides better accuracy than both the conventional intensity-based non-rigid registration algorithms for evaluating response of cervical cancer to radiation therapy. CT images provide anatomical information for radiation therapy evaluation in cervical cancer. However, they suffer from poor soft tissue contrast. MR images present high soft tissue contrast compared to CT [24, 25]. Staring et al. scanned each patient five times, one scan each week[12]. Lu et al. reported that each patient was scanned six times, one scan as baseline and then every week of treatment [10]. In the current study, each patient usually underwent MR scans twice: before internal-beam radiation therapy, and about 4 weeks after internal-beam radiation therapy. Compared to the previous data set, we have a much longer interval data set that corresponds to the real condition of local medical institution.

For cervical cancer, the deformation of tumor and organ between different MR image acquisitions is subject to several errors, including possible mechanical misalignment, respiratory and cardiac motion, involuntary and voluntary patient motion [26, 27], and bladder and bowel filling differences [28]. To minimize these ambiguities, patients filled their bladder before scanning. The volume of bladder in MR is larger than other organs, which may cause the improved registration precision. The volume of rectum much smaller and the movement of rectum between each scanning are larger than rectum. These factors may decrease the registration precision of rectum. The results of the current study support the findings of Ma *et al.* [29]. They reported that larger tumors had a higher degree of overlap compared with small tumors.

The main difficulty for validating the accuracy of registration is that there is no gold standard nor data sets with a known ground truth [11]. In this study, the bladder and rectum were manually outlined on axial T2-weighted MRI for each image, and the registration quality was computed based on these data. The automatic and operator-independent registration evaluation methods could provide a more objective and precise measurement of the misregistration [30].

One of the limitations of the present study was the relatively small cohort size. However, patient and tumor characteristics were diverse. These patients' mean age was 51.6, range from 33-66. The FIGO stages of the patients included in the study were: IIA, IIB, IIIA, and IIIB. The primary tumor MR volumes spread from 6.60 to 109.88 cc. A larger case is required for a more detailed investigation in future. And though the bladder and rectum were manually outlined by an experienced radiologist, there remains a number of uncertainties in areas of the bladder and rectum.

CONCLUSION

In this work, a nonrigid cervical MR image registration method using compact hybrid feature on α-MI is proposed. It effectively captures different tissues by a uniform feature space with compact formation. Promising results were obtained using clinical cervical MR images with long time internal between two imaging times which are consistent with the actual medical condition in local region. Furthermore, our proposed method is mainly based on robust fundamentals (DoG, SIFT, PCA), which can guarantee the valid range and reproducibility of the proposed registration method.

ACKNOWLEDGEMENTS

We sincerely thank Jennifer Wilson for her great help with language correction of the paper. This research is sponsored by National Natural Science Foundation of China (No. 61561002), 'Image and Intelligent Information Processing Innovation Team' the State Ethnic Affairs Commission Innovation Team, Ningxia Institutions of Higher Learning Science Research Project (No. PY1606), Ningxia first-class discipline and scientific research projects

[Downloaded from ijrr.com on 2026-11-24]

[DOI: 10.18869/acadpub.ijrr.18.1.13]

(electronic science and technology) (No. NXYLXK2017A07), Ningxia Medical Imaging Clinical Research Center Innovation Platform Construction Project (No.2018DPG05006), General Research Project of North Minzu University (No.2019XYZJK03).

***Conflicts of interest*:** *Declared none.*

REFERENCES

1. Organization WH (2006) Comprehensive cervical cancer control: a guide to essential practice. *Geneva Switzerland Who,* ***14(4667)****: 1436.*
2. Engin G (2006) Cervical cancer: MR imaging findings before, during, and after radiation therapy. *European radiology,* ***16(2)****: 313-24.*
3. Zhang S, Xin J, Guo Q, Ma J, Ma Q, Sun H, *et al.* (2014) Defining PET tumor volume in cervical cancer with hybrid PET/MRI: a comparative study. *Nuclear medicine communications,* ***35(7)****: 712-9.*
4. Mikolajczyk K, Schmid C (2005) A Performance Evaluation of Local Descriptors. *IEEE Trans Pattern Anal Mach Intell,* ***27(10)****:1615-30.*
5. Cheung W, Hamarneh G (2009) n-SIFT: n-Dimensional Scale Invariant Feature Transform. *IEEE Transactions on Image Processing,* ***18(9)****: 2012-21.*
6. Sotiras A, Davatzikos C, Paragios N (2013) Deformable Medical Image Registration: A Survey. *IEEE Transactions on Medical Imaging ,****32(7)****:1153-90.*
7. Bondar L, Hoogeman MS, Vasquez Osorio EM, Heijmen BJ (2010) A symmetric nonrigid registration method to handle large organ deformations in cervical cancer patients. *Medical physics,* ***37(7)****: 3760-72.*
8. Ferris DG, Lawhead RA, Dickman ED, Holtzapple N, Miller JA, Grogan S, *et al.* (2001) Multimodal hyperspectral imaging for the noninvasive diagnosis of cervical neoplasia. *Journal of lower genital tract disease,* ***5(2)****: 65-72.*
9. Vasquez Osorio EM, Hoogeman MS, Bondar L, Levendag PC, Heijmen BJ (2009) A novel flexible framework with automatic feature correspondence optimization for non-rigid registration in radiotherapy. *Medical physics,* ***36(7)****: 2848-59.*
10. Lu C, Chelikani S, Jaffray DA, Milosevic MF, Staib LH, Duncan JS (2012) Simultaneous nonrigid registration, segmentation, and tumor detection in MRI guided cervical cancer radiation therapy. *IEEE transactions on medical imaging,* ***31(6)****: 1213-27.*
11. García-Arteaga JD, Kybic J (2007) Automatic landmark detection for cervical image registration validation. *Proceedings of SPIE - The International Society for Optical Engineering,* ***68(4)****: 948-60.*
12. Staring M, Heide UAvd, Klein S, Viergever MA, Pluim JPW (2009) Registration of Cervical MRI Using Multifeature Mutual Information Using Multifeature Mutual Information. *IEEE Transactions on Medical Imaging,****28(9)****: 1412 -21.*
13. Mikolajczyk K and Schmid C (2004) Scale & Affine Invariant Interest Point Detectors. *International Journal of Computer Vision,* ***60(1)****: 63-86.*
14. Lindeberg T (1998) Feature detection with automatic scale selection. *International Journal of Computer Vision,* ***30(2)****: 79-116.*
15. Lowe D (2004) Distinctive Image Features from Scale-Invariant Keypoints. *International Journal of Computer Vision,* ***60****: 91-110.*
16. Yan K and Sukthankar R (2004) PCA-SIFT: a more distinctive representation for local image descriptors. *Cvpr,* ***2(2)****: 506-13.*
17. Pluim J, Maintz J, Viergever M (2003) Mutual information based registration of medical images: A survey. *IEEE Transactions on Medical Imaging,* ***22(8)****: 986-1004.*
18. Russakoff D, Tomasi C, Rohlfing T, Maurer C, editors. Image Similarity Using Mutual Information of Regions. ECCV; 2004; Berlin: Springer.
19. Redmond C and Yukich J (1996) Asymptotics for Euclidean functionals with power weighted edges. *Stochastic Processes and their Applications,* ***61(2)****: 289-304.*
20. Hero A, Ma B, Michel O, Gorman J (2002) Applications of entropic spanning graphs. *IEEE Signal Processing Magazine,* ***19(5)****: 85-95.*
21. Sabuncu MR and Ramadge P (2008) Using Spanning Graphs for Efficient Image Registration. *IEEE Transactions on Image Processing,* ***17(5)****: 788-97.*
22. Neemuchwala H, Hero A, Zabuawala S, Carson P (2006) Image Registration Methods in High-Dimensional Space. *International Journal of Imaging Systems and Technolog,****16****: 130-45.*
23. Klein S, Staring M, Murphy K, Viergever M, Pluim J (2010) Elastix: a toolbox for intensity-based medical image registration. *IEEE Transactions on Medical Imaging,* ***29(1)****: 196 -205.*
24. Zhang S, Xin J, Guo Q, Ma J, Ma Q, Sun H (2014) Comparison of tumor volume between PET and MRI in cervical cancer with hybrid PET/MR. *International journal of gynecological cancer : official journal of the International Gynecological Cancer Society,* ***24(4)****: 744-50.*
25. Zaidi H and El Naqa I (2010) PET-guided delineation of radiation therapy treatment volumes: a survey of image segmentation techniques. *European journal of nuclear medicine and molecular imaging,* ***37(11)****: 2165-87.*
26. Rakheja R, DeMello L, Chandarana H, Glielmi C, Geppert C, Faul D, *et al.* (2013) Comparison of the accuracy of PET/CT and PET/MRI spatial registration of multiple metastatic lesions. *AJR American journal of roentgenology,* ***201(5)****: 1120-3.*
27. Cohade C, Osman M, Marshall LN, Wahl RN (2003) PET-CT: accuracy of PET and CT spatial registration of lung lesions. *European journal of nuclear medicine and molecular imaging,****30(5)****: 721-6.*
28. Brendle CB, Schmidt H, Fleischer S, Braeuning UH, Pfannenberg CA, Schwenzer NF (2013) Simultaneously acquired MR/PET images compared with sequential MR/PET and PET/CT: alignment quality. *Radiology,* ***268(1)****: 190-9.*
29. Ma DJ, Zhu JM, Grigsby PW (2011) Tumor volume discrepancies between FDG-PET and MRI for cervical cancer. *Radiotherapy and oncology : journal of the European Society for Therapeutic Radiology and Oncology,* ***98(1)****:139-42.*
30. Zhang S, Xin J, Sun H, Ma J, Ma Q, Guo Q, *et al.* (2016) Accuracy of PET/MR image coregistration of cervical lesions. *Nuclear medicine communications,* ***37(6)****: 609-15.*

[Downloaded from ijrr.com on 2026-11-24]

[DOI: 10.18869/acadpub.ijrr.18.1.13]